Proc. Natl. Acad. Sci. USA
Vol. 93, pp. 10763–10768, October 1996
Biophysics

Multiphoton fluorescence excitation: New spectral windows for biological nonlinear microscopy

CHRIS XU, WARREN ZIPFEL, JASON B. SHEAR*, REBECCA M. WILLIAMS, AND WATT W. WEBB

Applied Physics, Cornell University, Ithaca, NY 14853

Contributed by Watt W. Webb, July 16, 1996

ABSTRACT **Intrinsic, three-dimensionally resolved, microscopic imaging of dynamical structures and biochemical processes in living preparations has been realized by nonlinear laser scanning fluorescence microscopy. The search for useful two-photon and three-photon excitation spectra, motivated by the emergence of nonlinear microscopy as a powerful biophysical instrument, has now discovered a virtual artist's palette of chemical indicators, fluorescent markers, and native biological fluorophores, including NADH, flavins, and green fluorescent proteins, that are applicable to living biological preparations. More than 25 two-photon excitation spectra of ultraviolet and visible absorbing molecules reveal useful cross sections, some conveniently blue-shifted, for near-infrared absorption. Measurements of three-photon fluorophore excitation spectra now define alternative windows at relatively benign wavelengths to excite deeper ultraviolet fluorophores. The inherent optical sectioning capability of nonlinear excitation provides three-dimensional resolution for imaging and avoids out-of-focus background and photodamage. Here, the measured nonlinear excitation spectra and their photophysical characteristics that empower nonlinear laser microscopy for biological imaging are described.**

Molecular two-photon excitation (TPE) was predicted by Göppert-Mayer in 1931 (1). Experimental observations of multiphoton processes awaited the invention of pulsed ruby lasers in 1960. Closely following the demonstration of second-harmonic generation (SHG), the first demonstration of nonlinear optics, two-photon absorption was utilized by Kaiser and Garrett to excite fluorescence emission in $CaF_2:Eu^{3+}$ (2). Three-photon excited fluorescence was observed and the three-photon absorption cross section for naphthalene crystals was estimated by Singh and Bradley in 1964 (3). Subsequently, multiphoton excitation and fluorescence has been used in molecular spectroscopy of various materials (4–8).

A significant biological application of multiphoton excitation began with the invention of two-photon laser scanning microscopy (TPLSM) by Denk, Strickler, and Webb in 1990 (9). Originally devised for localized photochemical activation of caged biomolecules, TPE of photochemical polymer crosslinking also has provided a means for high-density three-dimensional optical data storage at 10^{12} bits/cm^3 (10).

This article on multiphoton excitation is motivated by the emergence of TPLSM as a powerful new microscopy for three-dimensionally resolved fluorescence imaging of biological samples (11, 12). The development of TPLSM has been propelled by rapid technological advances in laser scanning microscopy (LSM) (13), fluorescence probe synthesis, mode-locked femtosecond lasers (14, 15), and computational three-dimensional image reconstruction (16). Recently, three-photon excited fluorescence and its potential applications in imaging have also been reported for several fluorescent dyes (17–20). Effective implementation of nonlinear laser microscopy, however, requires knowledge of the photophysics of multiphoton excitation, especially the multiphoton excitation properties of fluorophores and biological molecules.

Nonlinear LSM gains several advantages from two- or three-photon excitation of fluorescence. Because the absorption increases quadratically or cubicly with the excitation intensity, the fluorescence (and potential photobleaching and photodamage related to fluorescence excitation) are all confined to the vicinity of the focal point. This spatial localization not only provides intrinsic three-dimensional resolution in fluorescence microscopy but also provides unprecedented capabilities for three-dimensionally localized photochemistry in subfemtoliter volumes, including photolytic release of caged effector molecules (9). Because two or three photons are absorbed for each transition event, a red or near-infrared laser is used to excite fluorophores that normally absorb in the UV or deep-UV region. Such a wavelength shift avoids many limitations of UV lasers and UV optics. Because wide-field *detection* is used in nonlinear microscopy, even multiply scattered fluorescence photons contribute equally to the image formation, in contrast with confocal microscopy, where the unscattered photons form the confocal image (21). This efficient detection of fluorescence photons, combined with the relatively deep penetration of IR excitation light in most biological preparations (22), enables nonlinear microscopy to image deep (>200 μm) into turbid biological specimens. In general, the background interference from Rayleigh and Raman scattering is negligible because multiphoton excited fluorescence occurs at a much shorter wavelength region than the excitation light. Thus, ultrasensitive measurements are possible, including detection of single dye molecules (23, 24) and low quantities of fluorogen-labeled neurotransmitters (25). Finally, in addition to background interference, photodamage to living cells by deep UV excitation has previously limited the use of imaging based on native fluorescence. Three-photon excited fluorescence provides the unique opportunity to excite intrinsic chromophores, such as amino acids, proteins, and neurotransmitters, using relatively benign excitation wavelengths accessible with commercially available near-IR lasers (26). The combination of two- and three-photon excited fluorescence microscopy extends the useful range of nonlinear laser microscopy.

A basic parameter of fluorescence is the fluorescence excitation cross section. Although one-photon absorption spectra are well documented for a wide range of molecules, little is known of two- or three-photon absorption spectra of biologically useful fluorophores (27). Furthermore, it is often difficult to predict multiphoton excitation spectra, especially two-photon spectra, from the one-photon data because of differences in selection rules and the effects of vibronic coupling. We report measurements of two- and three-photon fluorescence excitation cross sections of biological indicators

The publication costs of this article were defrayed in part by page charge payment. This article must therefore be hereby marked "*advertisement*" in accordance with 18 U.S.C. §1734 solely to indicate this fact.

Abbreviation: TPE, two-photon excitation; LSM, laser scanning microscopy; TPLSM, two-photon LSM; GM, Göppert-Mayer; DiI, 1,1-dioctadecyl-3,3,3′,3′-tetramethylindocarbocyanine perchlorate; GFP, green fluorescent protein; DAPI, 4′,6-diamidino-2-phenylindole; n.a., numerical aperture; FWHM, full width at half maximum.

*Present address: Department of Chemistry, University of Texas, Austin, TX 78712.

and native chromophores. Detailed methods for obtaining the multiphoton excitation cross sections and spectra were reported elsewhere (28, 29). The potential of three-photon excited fluorescence in LSM is also demonstrated.

Two-Photon Excitation

Fig. 1*a* summarizes results of measurements of two-photon fluorescence excitation spectra [$\sigma_2(\lambda)$] of common fluorophores in the spectral range of 690-1050 nm. TPE spectra of various Ca^{2+} indicators are reported in Fig. 1*b*. TPE cross-section measurements of fluorescein, rhodamine B, and 1,1-dioctadecyl-3,3,3′,3′-tetramethylindocarbocyanine perchlorate (DiI) are shown in Fig. 2, with their corresponding one-photon absorption spectra. For comparison, the tuning ranges of several mode-locked laser sources are also plotted in Fig. 1. These spectra show that nonlinear fluorescence microscopy based on TPE can be expected to work well with most existing fluorophores and many available laser sources. For nonratiometric Ca^{2+} indicators, such as calcium crimson, calcium orange, and calcium green-1, we found that the TPE spectra of the Ca^{2+}-free and Ca^{2+}-bound forms are indistinguishable. The ratios of fluorescence intensity for the Ca^{2+}-free to Ca^{2+}-bound forms of these indicators are also comparable to their reported one-photon values.

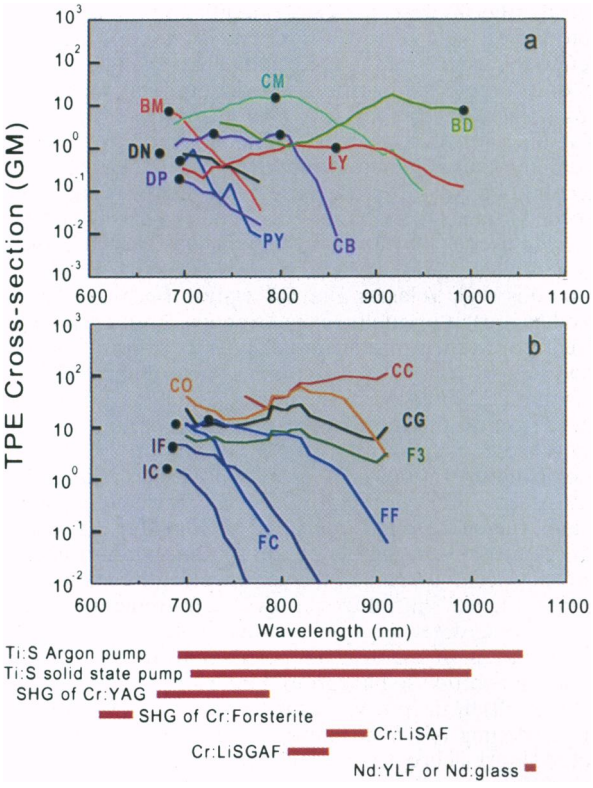

FIG. 1. Two-photon fluorescence excitation spectra of fluorophores. For BM (Bis-MSB), data represent two-photon absorption cross sections. For all the other fluorophores, data represent two-photon action cross sections—i.e., the product of the fluorescence emission quantum efficiencies and the two-photon absorption cross sections. Units are Göppert-Mayer (GM); 1 GM = 10^{-50} $cm^4 \cdot s$/photon. Spectra are excited with linearly polarized light using a mode-locked Ti:sapphire laser. Black dot indicates twice the wavelength of the one-photon absorption maximum of the fluorophore. For comparison, the tuning range of conveniently available mode-locked laser sources are also plotted. The fluorophores illustrated in *a* are as follows: BM, *p*-bis(*o*-methylstyryl)benzene; CB, Cascade Blue hydrazide trisodium salt; LY, Lucifer yellow CH ammonium salt; BD (Bodipy), 4,4-difluoro-1,3,5,7,8-pentamethyl-4-bora-3*a*,4*a*-diazaindacene-2,6-disulfonic acid disodium salt; DP, (DAPI not DNA bound) 4′,6-diamidino-2-phenylindole dyhydrochloride; DN (dansyl), 5-dimethylaminonaphthalene-1-sulfonyl hydrazine; PY, 1,2-bis-(1-pyrenedecanoyl)-*sn*-glycero-3-phosphocholine; and CM, coumarin 307. The fluorophores illustrated in *b* are as follows: IC, indo-1 with Ca^{2+}; IF, indo-1 without Ca^{2+}; FC, fura-2 with Ca^{2+}; FF, fura-2 without Ca^{2+}; CG, calcium green-1 with Ca^{2+}; CO, calcium orange with Ca^{2+}; CC, calcium crimson with Ca^{2+}; and F3, fluo-3 with Ca^{2+}. All of the samples were purchased from either Eastman Kodak or Molecular Probes. Note that logarithmic scales were used.

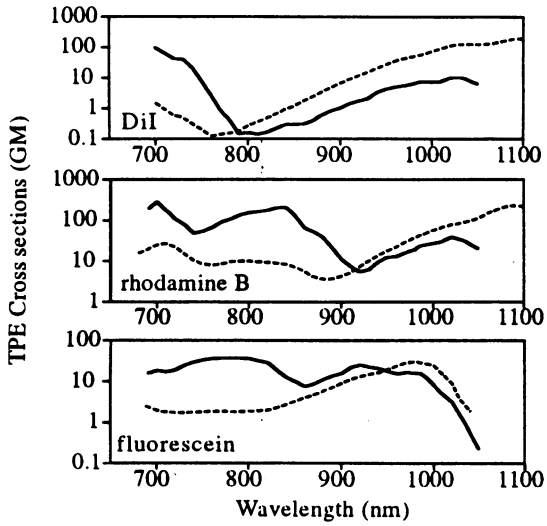

FIG. 2. Comparison of one-photon (broken lines) and two-photon (solid lines) fluorescence excitation spectra of rhodamine B, fluorescein (pH ≈ 13), and DiI. The *y*-axis values represent two-photon absorption cross sections for rhodamine B and fluorescein, and two-photon action cross sections for DiI. For the one-photon results, the *x*-axis values represent twice the one-photon transition wavelengths. The one-photon results are plotted in arbitrary scale.

Green fluorescent proteins (GFPs) have attracted tremendous interest as biological reporters for gene expression (30). Images of cultured cells using two-photon excited GFP fluorescence have been reported recently (31). Wild-type GFPs have high UV absorption at 400 nm and relatively low visible absorption at 480 nm. To facilitate the use of GFPs with visible excitation, mutant S65T (replacement of Ser-65 with Thr) was engineered to enhance the visible absorption band (32). We have measured the TPE spectra of GFP wild type and the GFP S65T mutant. Shown in Fig. 3, both TPE spectra are similar to the corresponding one-photon spectra. Thus, these results indicate that wild-type GFP can be two-photon excited using the same wavelength needed to excite UV and visible fluorophores (Figs. 1 and 2); while only long-wavelength visible fluorophores can be simultaneously excited with the S65T mutant.

Two-photon excited cellular autofluorescence from intrinsic chromophores such as NAD(P)H has been used to study the cellular metabolic state (33). Photodamage of cells can also be detected by monitoring autofluorescence changes. However, for most fluorescence imaging applications, autofluorescence background is undesirable, as it limits the detection sensitivity for fluorescent probes. Thus, knowledge of the TPE spectra of NADH and flavins should help to optimize TPE fluorescence imaging and may also provide insight to the photodamage mechanisms of living biological preparations in the near infrared (34). We report in Fig. 4 measurements of the TPE spectra of NADH and FMN. Results for NADPH are nearly identical to those for NADH. The TPE spectrum of FAD is similar to that of FMN, although the action cross sections of FAD are approximately 1/9 as large as those of FMN (presumably due to quenching of fluorescence by the adenine).

One general feature conserved in all measured TPE spectra is that the TPE peak absorption wavelengths never appear red

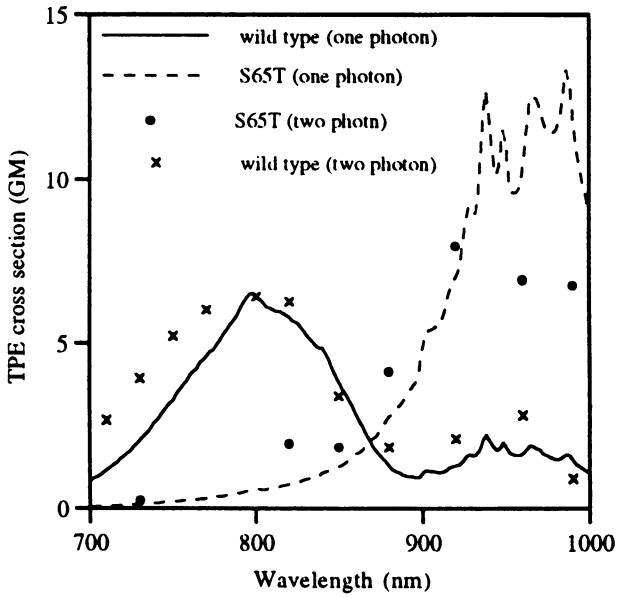

FIG. 3. Two-photon action cross sections of GFPs. The *y*-axis values represent two-photon action cross sections for GFPs. For the one-photon results, the *x*-axis values represent twice the one-photon transition wavelengths. The one-photon results are plotted in arbitrary scale. GFPs were provided by George Patterson and David W. Piston, Vanderbilt University.

shifted (but are frequently blue shifted) relative to twice the one-photon absorption peaks. For example, large blue shifts were observed for rhodamine B, DiI, fluorescein, and several Ca^{2+} indicators (Fig. 2). Although these interesting spectral features still are not understood quantitatively, there are several desirable consequences of such significant blue shifts. First, the resolution of TPLSM using these fluorophores is considerably higher than predicted by assuming TPE peak wavelengths at twice the one-photon absorption peak wavelengths. Second, the blue shifts allow conveniently available mode-locked laser sources to excite popular dyes as indicated in Figs. 1 and 2. Finally, a number of conventional dyes with disparate one-photon absorption spectra can be excited by TPE at a single wavelength. This capability, combined with the large spectral separation between the excitation light and the fluorescence light, greatly simplifies experiments requiring multiple fluorophores. We show in Fig. 5 simultaneous excitation of rhodamine, 4′,6-diamidino-2-phenylindole (DAPI), pyrene, and Bodipy at 705 nm.

Fluorescence resonance energy transfer (FRET) is a powerful tool for measuring intermolecular distances (35). The

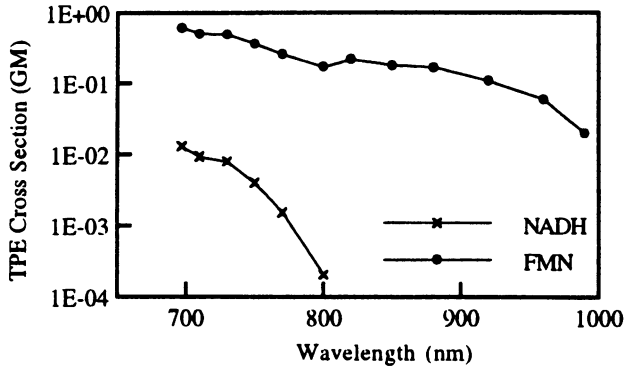

FIG. 4. Two-photon action cross sections of the native fluorophores NADH and FMN. NADH and FMN were purchased from Sigma.

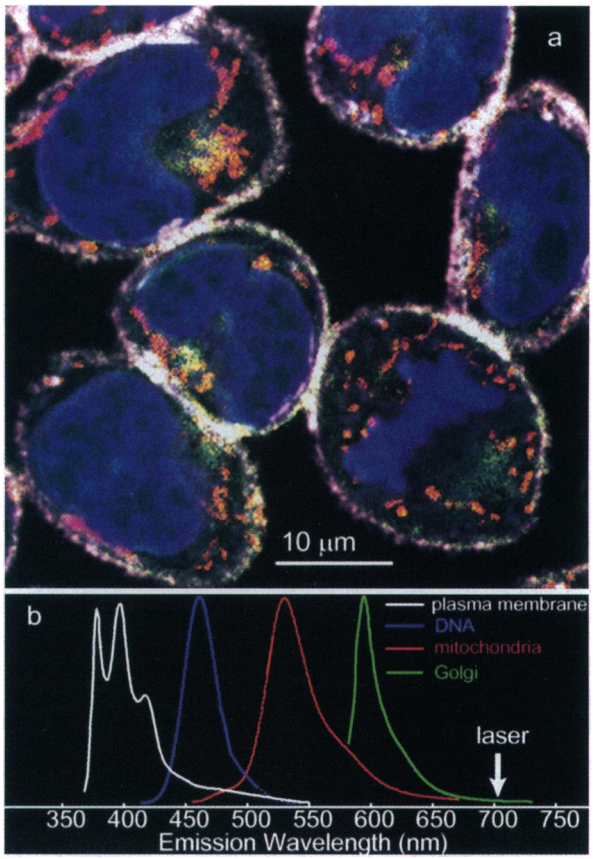

FIG. 5. (*Upper*) Four-color staining of plasma membrane, nuclei, Golgi complex, and mitochondria in rat basophilic leukemia (RBL) cells visualized with two-photon illumination. RBL cells were incubated with four different stains: a plasma membrane label (pyrene lysophosphatidylcholine), a nuclear stain (DAPI), a Golgi label (Bodipy sphingomyelin), and a mitochondrial stain (rhodamine 123). The image was obtained by using a modified Bio-Rad MRC-600 confocal microscope to scan the excitation beam (705 nm, ≈120-fs pulsewidth, 1–5 mW at the sample) through a ×40/numerical aperture (n.a.) 1.3 oil-immersion objective. Epifluorescence was collected by using nondescanned external detection into four channels: 400 nm, 30 nm full width at half maximum (FWHM) (pyrene fluorescence, white); 440 nm, 50 nm FWHM (DAPI fluorescence, blue); 530 nm, 30 nm FWHM (rhodamine 123 fluorescence, red/orange) and 580 nm, 30 nm FWHM (Bodipy fluorescence, green). (*Lower*) Approximate emission spectra of the dyes used (color coded as in the image) and the excitation laser wavelength.

applicability of FRET depends on the overlap of fluorescence emission and excitation spectra of the donor and acceptor. We have found no significant fluorescence emission spectra difference between one- and two-photon excitation for the fluorophores investigated in our experiments (28). Knowledge of the TPE spectra also provides new capabilities by combining FRET with TPE. For example, the optimal excitation wavelength of TPE FRET using fluorescein and rhodamine is ≈920 nm (Fig. 2). Significantly better choices of donor and acceptor in TPE FRET would be fluorescein and DiI when excited at ≈790 nm, where the fluorescein TPE cross section is approximately 10^2 times larger than DiI (Fig. 2).

Three-Photon Excitation

Very recently, unexpectedly large three-photon absorption cross sections (with $\sigma_3 \approx 10^{-75}$ cm^6·s^2) have been reported (36, 37). The discoveries of such large cross sections are promising. We have observed and measured three-photon excited fluorescence from UV fluorophores, including Ca^{2+} indicators fura-2 and indo-1, DNA stain DAPI, and the fluorescent

Table 1. One-, two-, and three-photon excitation cross sections (σ)

Fluorophore	σ_1 (at λ nm), 10^{-16} cm^2	$\eta\sigma_2$ (at 700 nm), 10^{-50} cm^4·s per photon	$\eta\sigma_3$ (at 1.0 μm), 10^{-83} cm^6·s^2 per photon^2
DAPI*	1.3 (345 nm)	0.16	0.25
Dansyl	0.17 (336 nm)	1	0.3
Fura-2 + Ca^{2+}	1.2 (335 nm)	12	30
Fura-2 free	1.0 (362 nm)	11	20
Indo-1 + Ca^{2+}	1.3 (340 nm)	1.5	6
Indo-1 free	1.3 (345 nm)	3.5	2

Cross sections were measured in 10^{-4} M solution. η is the fluorescence quantum efficiency. We have assumed that two- and three-photon fluorescence quantum efficiencies are the same. The estimated uncertainties are 30% for the two-photon cross sections and about factor of 3 for the three-photon cross sections.
*DAPI not bound to DNA. The fluorescence quantum efficiency of DAPI is expected to go up by 20-fold upon binding to DNA (38).

reagent dansyl hydrazine, by excitation at $\lambda \approx 1.0$ μm. The approximate three-photon cross sections (σ_3) are listed in Table 1. For a comparison, the corresponding one- and two-photon cross sections are also given.

To investigate the photophysics of three-photon excitation of fluorophores, we have measured several three-photon excitation spectra [$\sigma_3(\lambda)$] from 960 to 1050 nm for comparison with one-photon excitation spectra (Fig. 6). The qualitative agreement shown in Fig. 6 suggests that these three-photon excitation spectra parallel the corresponding one-photon excitation spectra as expected because the same initial excited states can be reached via one- or three-photon excitation without violating any selection rules. Three-photon excited fluorescence emission spectra of several fluorophores were also measured. We found no difference between two- and three-photon excited fluorescence, which indicates the same fluorescent state is reached regardless of the excitation mode. Previously we have observed no difference between the emission spectra of one- and two-photon excited fluorescence (28, 29), suggesting that quite generally the same fluorescent states are reached by nonlinear and linear excitation.

To demonstrate the imaging capability of three-photon excited fluorescence, chromosomes in a rat basophilic leukemia (RBL) cell stained with DAPI were imaged in a laser scanning microscope at $\approx$1.0 μm (Fig. 7), and compared with two-photon microscopy, which also provides excellent (virtually indistinguishable) images in this application (12). The longer wavelengths required for three-photon excitation should slightly decrease laser microscopy resolution; for the imaging conditions of Fig. 7, the calculated FWHM of the fluorescence distribution of a point source resulting from three-photon excitation at 1.05 μm is $\approx$0.24 μm in the focal plane and 0.73 μm along the optical axis, while the corresponding numbers for TPE at 700 nm are $\approx$0.2 μm and $\approx$0.6 μm (39). However, there is a compensating image enhancement because the signal-to-background ratio (S/B) (40) of a three-photon microscope is theoretically equivalent to application of an ideal confocal spatial filter in TPLSM. In a uniform fluorescent sample, for example, if we define signal as fluorescence from a volume that is within the FWHM of the fluorescence distribution and background as fluorescence from outside that volume, the resulting S/B values for two- and three-photon excitation are 0.32 and 0.45, respectively. When S/B is taken into account, the effective resolutions of two- and three-photon fluorescence microscopy should be comparable.

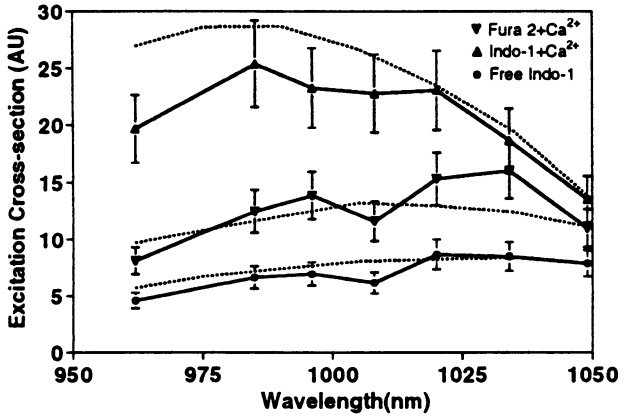

FIG. 6. Comparison of one-photon (broken lines) and three-photon (solid lines) fluorescence excitation of indo-1 and fura-2. For the one-photon results, the x-axis values represent 3 times the one-photon transition wavelengths. The one-photon results are normalized to their corresponding three-photon data at 1050 nm.

Consequences of the Photophysics of Multiphoton Excitation

The applicability of nonlinear microscopy depends crucially on the two- and three-photon fluorescence excitation cross sections of various fluorophores and biomolecules. A simple estimation of multiphoton excitation cross sections can be obtained by using the appropriate order perturbation theory (41). Intuitively, multiphoton processes require two or more photons to interact *simultaneously* with the molecule. The "cross-sectional" area (A) of a molecule can be estimated by its dipole transition length (typically $A \approx 10^{-16}$ to 10^{-17} cm^2 for a transition length of 10^{-8} to 10^{-9} cm). The time scale for photon coincidence is determined by the lifetimes of the virtual intermediate states $\Delta\tau \approx 10^{-16}$ s (estimated from the uncertainty principle). Hence, the expected TPE cross sections (σ_2) are approximately 10^{-49} cm^4·s per photon (i.e., $A^2\Delta\tau$). Correspondingly, the three-photon excitation cross sections are expected to be $\sigma_3 \approx 10^{-82}$ cm^6(s/photon)^2 (i.e., $A^3\Delta\tau^2$). Table 1 and Fig. 1 show that these estimates are in qualitative agreement with our experimental data.

The maximum fluorescence output available for image formation is obtained by using ultrashort pulsed excitation. However, fluorescence saturates at the limit of one transition per pulse per fluorophore. For an n-photon process, fluorescence output per excitation pulse is proportional to $\sigma_n I_{peak}^n \tau$,

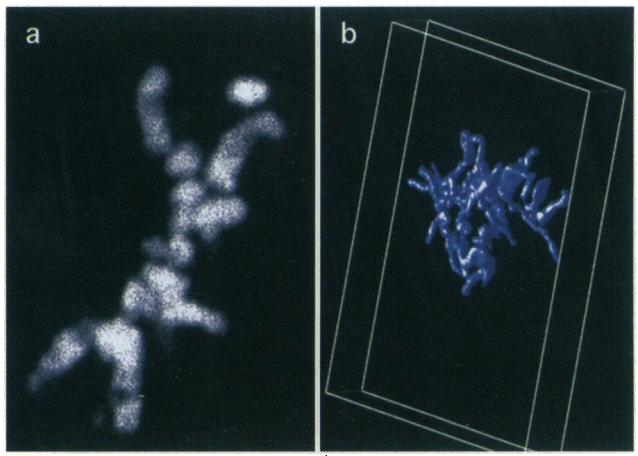

FIG. 7. (*a*) One section from a z series through a dividing RBL cell stained with DAPI. The image was collected as in Fig. 5, except that excitation wavelength was 1000 nm (120-fs pulsewidth) and only one collection channel was used without an emission filter. The image is $\approx$15 by 20 μm and is a Kalman average of four scans (1 s acquisition time per frame). (*b*) Isosurface rendering of 50 sections through a dividing RBL cell stained with DAPI. Reconstruction was carried out using the IBM Data Explorer software package on an RS-6000 workstation.

where I_{peak} is the peak intensity (28), σ_n is the n-photon cross section, and τ is the pulse width. For a square pulse in time, saturation occurs when $\sigma_n I_{peak}^n \tau \approx 1$. Therefore, the saturation peak intensity for the n-photon process (I_{ns}) is simply

$$I_{ns} \approx (\sigma_n \tau)^{-1/n}. \quad [1]$$

Using diffraction limited focusing geometry, the relation between the average incident photon flux (P_{avg}, in units of photons/s) and I_{peak} is approximately

$$P_{avg} \approx \frac{(0.61)^2 \lambda^2 (f \cdot \tau) I_{peak}}{(\text{n.a.})^2}, \quad [2]$$

where f is the pulse repetition rate. Combining Eqs. **1** and **2**, saturation power for the n-photon process ($P_{avg}^{(ns)}$) can be estimated as

$$P_{avg}^{(ns)} \approx \frac{(0.61)^2 \lambda^2 (f \cdot \tau)}{(\text{n.a.})^2 \, (\sigma_n \cdot \tau)^{-1/n}}. \quad [3]$$

With a high-n.a. (1.3) objective lens and a mode-locked Ti:sapphire laser providing 100-fs pulses at 80-MHz repetition rate and 1.0-μm excitation wavelength, the estimated saturation powers for two-, three-, and four-photon processes are, respectively, ≈30 mW, ≈150 mW, and ≈300 mW by Eq. **3** and the excitation cross sections estimated above. Although these incident power levels are easily available from femtosecond laser sources such as the mode-locked Ti:sapphire laser, solvent dielectric breakdown may occur before saturation is reached in three- and four-photon excitation.

The ratio (r) of three- to two-photon excited fluorescence emission scales as $r \sim \sigma_3(\lambda) I_{peak} / \sigma_2(\lambda)$. Hence, a measurable combination of two- and three-photon excited fluorescence is expected within certain wavelength and intensity ranges. This is shown for the case of fura-2. For this excitation ratiometric calcium indicator, the one-photon absorption maximum of fura-2 shifts from 362 nm in the Ca^{2+}-free form to 335 nm on binding to Ca^{2+} (42), and the corresponding shifts are also apparent in its two-photon fluorescence excitation spectra (Fig. 1*b*). This absorption change makes the ratio between three- and two-photon excited fluorescence of the two species quite different. At $I_{peak} \approx 10^{30}$ photons/(cm^2·s), we found that for the Ca^{2+}-bound species, TPE dominates at $\lambda < 830$ nm and three-photon dominates at $\lambda > 900$ nm; while for the Ca^{2+}-free species, two-photon dominates up to 910 nm and three-photon dominates only at $\lambda > 960$ nm. At intermediate wavelengths, a mixture of two- and three-photon excitation is observed. Table 2 lists the measured power exponents for excitation of fura-2 at several wavelengths, which shows the gradual transition from two-photon to three-photon excitation. Although the three-dimensional imaging capability is preserved in this wavelength range, quantitative imaging, as is required in calcium measurements using ratiometric indicators, will be complicated by the dependence of calibration on incident intensities.

Table 2. Slopes in the logarithmic plot of fluorescence output versus incident intensity at selected wavelengths

	Slope					
Fluorophore	838 nm	861 nm	880 nm	900 nm	922 nm	970 nm
Fura-2 + Ca^{2+}	2.2	2.4	2.6	2.7	2.9	3.0
Fura-2 free	2.0	2.0	2.0	2.1	2.3	2.9

Slopes were measured at $I_{peak} \approx 10^{30}$ photons/(cm^2·s). A slope between 2.0 and 3.0 indicates that a mixture of two- and three-photon excited fluorescence was generated. The uncertainties in the slopes are ≈6%.

An interesting difference between two- and three-photon fluorescence excitation is the dependence on the excitation beam waist size or the n.a. of the focusing lens. Assuming a Gaussian–Lorentzian beam profile and a sample thickness that is much greater than the Raleigh length of the Gaussian beam (i.e., thick sample limit), the appropriate form for the fluorescence emission rate resulting from three-photon excitation, $\langle F(t) \rangle$,is

$$\langle F(t) \rangle \propto \sigma_3 \frac{P_{avg}^3}{(f \cdot \tau)^2 w_0^2}, \quad [4]$$

where w_0 is the Gaussian beam waist. A similar expression can also be obtained for diffraction-limited focus, $\langle F(t) \rangle \propto \sigma_3 (\text{n.a.})^2 P_{avg}^3 / (f \cdot \tau)^2$. We note that $\langle F(t) \rangle$ depends on the n.a. of the focusing lens [or the beam waist radius (Eq. **4**)], in contrast to TPE, where $\langle F(t) \rangle$ is independent of n.a. in the same thick sample limit (28, 43). Thus, one can increase or decrease the relative contribution of two-photon (or three-photon) excitation by manipulating the excitation pulse width and focal spot size (Eq. **2**). This property may become useful if higher- (more than second-) order excitation processes, such as three-photon excitation of amino acids and nucleic acids, contribute significantly to the photodamage of biological specimens.

Intersystem crossing and photobleaching properties of one-, two-, or three-photon excitation of the fluorophores are expected to be the same if the same excited state is reached. Experimentally, intersystem crossing and photobleaching cause severe deviation from the expected power law dependence of the excited fluorescence. Photobleaching may account for the nonquadratic dependence of TPE fluorescence in some earlier reports (44). Using a high-n.a. water immersion objective lens (n.a. = 1.2), we have observed no significant deviation from the cubic dependence at I_{peak} up to 6×10^{30} photons/(cm^2·s) for three-photon excitation of fura-2 and DAPI at 992 nm. Dramatic decreases in the apparent power exponent were observed at photon flux density higher than 10^{31} photons/(cm^2·s) for both fluorophores. Although intersystem crossing and photobleaching may account for such deviation, other factors, such as field-induced changes in the electronic properties of the fluorophores, may become important at very high intensities (7). The instantaneous electric field (E) at the focal spot is approximately 3×10^7 V/cm at $I_{peak} = 10^{31}$ photons/(cm^2·s), which is probably sufficient to modify the photophysical properties of the dye molecules.

Another possible concern at such high instantaneous field strengths is dielectric breakdown of the solvent. A previously measured breakdown threshold field strength for water is 1.6×10^{12} W/cm^2 (≈2×10^7 V/cm) when 30-psec pulses at 1.06 μm are used (45). However, the breakdown threshold is expected to be considerably higher (>10^{13} W/cm^2 or >5×10^7 V/cm) when 100-fs pulses are used (46–48). We note that peak intensities are generally less than 4×10^{11} W/cm^2 and 2×10^{12} W/cm^2 in typical two- and three-photon microscopy, respectively. Thus, the peak intensities in routine TPLSM are significantly below the dielectric breakdown threshold, but dielectric breakdown may be possible during high-intensity three-photon excitations. It will be interesting to compare intersystem crossing and photobleaching properties resulting from one-, two-, and three-photon excitation of fluorophores.

Prospectives

We have reported two- and three-photon fluorescence excitation spectra of the most common biological fluorophores in the tuning range of a mode-locked Ti:sapphire laser. In combination with earlier applications (9, 12, 33, 43), these spectra show that nonlinear fluorescence microscopy based on TPE can be expected to work well with available and forth-

coming solid-state laser sources for most existing fluorophores, including fluorophores normally excitable only in the UV region. Our measured three-photon fluorescence excitation cross sections and images have shown the feasibility of three-photon fluorescence microscopy for special applications and suggested further opportunities (26). Although three-photon microscopy requires 5–10 times higher incident power than in TPLSM to obtain a comparable fluorescence excitation rate, it does provide alternative wavelength windows to probe biological specimens, especially in the deep-UV region. The significance of such a wavelength option depends on the laser availability and the possible photodamage mechanism for various applications. In general, the wavelength dependence and mechanisms of photodamage to living cells are largely unknown with either single or multiphoton excitation and appear to vary greatly in various preparations. However, because multiphoton excitation is confined to the focal plane, it spatially limits photodamage. Substantial research is currently directed toward elucidating the photodamage mechanisms. Although it remains to map the full scope of three-photon excitation as a useful complement to the existing TPLSM, our reported nonlinear excitation spectra, combined with future information on the photodamage mechanisms, should guide various biological applications yet to be explored.

The authors acknowledge helpful facilities of Cornell Material Science Center and the National Institutes of Health Parallel Processing Resource for Biomedical Scientists at Cornell Theory Center. They also acknowledge fruitful discussions with J. Mertz, J. Guild, and S. Maiti. This work was carried out in the Developmental Resource for Biophysical Imaging and Opto-electronics with funding by the National Science Foundation (DIR8800278) and the National Institutes of Health (RR04224 and RR07719). J.S. is a National Science Foundation Postdoctoral Fellow supported by Grant CHE-9403174.

1. Göppert-Mayer, M. (1931) *Ann. Phys.* **9,** 273–295.
2. Kaiser, W. & Garrett, C. G. B. (1961) *Phys. Rev. Lett.* **7,** 229–231.
3. Singh, S. & Bradley, L. T. (1964) *Phys. Rev. Lett.* **12,** 612–614.
4. Pantell, R., Pradere, F., Hanus, J., Schott, M. & Puthoff, H. (1966) *J. Chem. Phys.* **46,** 3507–3511.
5. Shreve, A. P. & Albrecht, A. C. (1990) *J. Chem. Phys.* **94,** 5772–5773.
6. McClain, W. M. & Harris, R. A. (1977) in *Excited States*, ed. Lim, E. C. (Academic, New York), pp. 1–56.
7. Birge, R. R. (1983) in *Ultrasensitive Laser Spectroscopy*, ed. Kliger, D. S. (Academic, New York), pp. 109–174.
8. Shreve, A. P., Trautmen, J. K., Owens, T. G. & Albrecht, A. C. (1990) *Chem. Phys. Lett.* **170,** 51–56.
9. Denk, W., Strickler, J. H. & Webb, W. W. (1990) *Science* **248,** 73–76.
10. Strickler, J. H. & Webb, W. W. (1991) *Opt. Lett.* 1780–1782.
11. Yuste, R. & Denk, W. (1995) *Nature (London)* **375,** 682–684.
12. Williams, R. M., Piston, D. W. & Webb, W. W. (1994) *FASEB J.* **8,** 804–813.
13. Wilson, T. & Sheppard, C. J. R. (1984) *Theory and Practice of Scanning Optical Microscopy* (Academic, New York).
14. Valdmanis, J. A. & Fork, R. L. (1986) *IEEE J. Quantum Electron.* **QE-22,** 112–118.
15. Spence, D. E., Kean, P. N. & Sibbett, W. (1991) *Opt. Lett.* **16,** 42–44.
16. Garrity, M. (1990) *Comput. Graphics* **24,** 35–40.
17. Gryczynski, I., Szmacinski, H. & Lakowicz, J. R. (1995) *Photochem. Photobiol.* **62,** 804–808.
18. Gryczynski, I., Szmacinski, H. & Lakowicz, J. R. (1995) *Chem. Phys. Lett.* **245,** 30–35.
19. Xu, C., Zipfel, W. & Webb, W. W. (1996) *Biophys. J.* **70,** A429.
20. Wokosin, D. L., Centonze, V. E., Crittenden, S. & White, J. G. (1995) *Mol. Biol. Cell* **6,** 113a.
21. Schmitt, J. M., Knuttel, A. & Yadlowsky, M. (1994) *J. Opt. Soc. Am. A* **11,** 2226–2235.
22. Duck, F. A. (1990) *Physical Properties of Tissue* (Academic, London).
23. Mertz, J., Xu, C. & Webb, W. W. (1995) *Opt. Lett.* 2532–2534.
24. Plakhotnik, T., Walser, D., Pirotta, M., Renn, A. & Wild, U. P. (1996) *Science* **271,** 1703–1705.
25. Shear, J. B., Brown, E. B. & Webb, W. W. (1996) *Anal. Chem.* **68,** 1778–1783.
26. Maiti, S., Shear, J. B. & Webb, W. W. (1996) *Biophys. J.* **70,** A210.
27. Smith, W. L. (1986) in *Handbook of Laser Science and Technology*, ed. Weber, J. (CRC, Baca Raton, FL), pp. 229–258.
28. Xu, C. & Webb, W. W. (1996) *J. Opt. Soc. Am. B* **13,** 481–491.
29. Xu, C., Guild, J., Webb, W. W. & Denk, W. (1995) *Opt. Lett.* **20,** 2372–2374.
30. Chalfie, M., Tu, Y., Euskirchen, G., Ward, W. W. & Prasher, D. C. (1994) *Science* **263,** 802–805.
31. Niswender, K. D., Blackman, S. M., Rohde, L., Magnuson, M. A. & Piston, D. W. (1995) *J. Microsc.* **180,** 109–116.
32. Cubitt, A. B., Heim, R., Adams, S. R., Boyd, A. E., Gross, L. A. & Tsien, R. Y. (1995) *Trends Biochem. Sci.* **20,** 448–455.
33. Piston, D. W., Masters, B. R. & Webb, W. W. (1995) *J. Microsc.* **178,** 20–27.
34. Konig, K., Liu, Y., Sonek, G. J., Berns, M. & Tromberg, B. J. (1995) *Photochem. Photobiol.* **62,** 830–835.
35. Stryer, L. (1978) *Annu. Rev. Biochem.* **47,** 819–846.
36. Davey, A. P., Bourdin, E., Henari, F. & Blau, W. (1995) *Appl. Phys. Lett.* **67,** 884–885.
37. He, G. S., Bhawalkar, J. D. & Prasad, P. N. (1995) *Opt. Lett.* **20,** 1524–1526.
38. Haugland, R. P. (1992) *Handbook of Fluorescent Probes and Research Chemicals* (Molecular Probes, Eugene, OR), 5th Ed., p. 222.
39. Sheppard, C. J. R. & Gu, M. (1990) *Optik* **86,** 104.
40. Sandison, D. R. & Webb, W. W. (1994) *Appl. Opt.* **33,** 603–615.
41. Faisal, F. H. M. (1987) *Theory of Multiphoton Processes* (Plenum, New York).
42. Grynkiewicz, G., Poenie, M. & Tsien, R. Y. (1985) *J. Biol. Chem.* **260,** 3440–3450.
43. Denk, W., Piston, D. W. & Webb, W. W. (1995) in *The Handbook of Confocal Microscopy*, ed. Pawley, J. (Plenum, New York), pp. 445–458.
44. Fischer, A., Cremer, C. & Stelzer, E. H. K. (1995) *Appl. Opt.* **34,** 1989–2003.
45. Smith, W. L., Liu, P. & Bloembergen, N. (1977) *Phys. Rev. A* **15,** 2396–2403.
46. Smith, W. L. (1978) *Opt. Eng.* **17,** 489–503.
47. Du, D., Liu, X., Squier, K. J. & Mourou, G. (1994) *Appl. Phys. Lett.* **64,** 3071–3073.
48. Stuart, B. C., Feit, M. D., Rubenchik, A. M., Shore, B. W. & Perry, M. D. (1995) *Phys. Rev. Lett.* **74,** 2248–2251.